International Communications in Heat and Mass Transfer 56 (2014) 15–24

Contents lists available at ScienceDirect

International Communications in Heat and Mass Transfer

journal homepage: www.elsevier.com/locate/ichmt

Modulated heat transfer tube with mesh cylinder inserted ☆

Feng Xing [a,b], Jian Xie [a,b], Jinliang Xu [a,*]

[a] State Key Laboratory of Alternate Electrical Power System with Renewable Energy Sources, North China Electric Power University, Beijing 102206, China
[b] The Beijing Key Laboratory of Multiphase Flow and Heat Transfer, North China Electric Power University, Beijing 102206, China

ARTICLE INFO

Available online 9 May 2014

Keywords:
Flow field modulation
Mesh cylinder
Heat transfer enhancement

ABSTRACT

The concept of flow field modulation was proposed to enhance convective heat transfer in tubes. A mesh cylinder is suspended in the tube, dividing the cross section into an annular region and a core region. When the fluid flows over the mesh screen, a small portion of flow penetrates into the core region through mesh pores, while most of the fluid is within the annular region, leading to larger velocity gradient near the wall than that for the bare tube without mesh cylinder, this large velocity gradient can result in significant heat transfer enhancement. In this study experiments were performed at constant heat flux boundary conditions with water as the working fluid. Reynolds numbers vary from 2109 to 20,175, covering the transition and turbulent flow regimes. Experimental results showed that the heat transfer was enhanced over the whole length of tube, with the enhancement ratios from 1.21 to 1.84, and the largest enhancement ratio occurred in the transition flow regime. The mechanism for heat transfer enhancement could be attributed to: (1) The multi-scale characteristics of the heat transfer tube; (2) The modulated flow field with larger velocity and velocity gradient near the wall; and (3) The enhanced flow turbulence intensity.

1. Introduction

Heat exchangers have wide applications in various industry sectors. The design of heat exchangers is complicated, as it needs accurate analysis on heat transfer rate and pressure drop for long-term reliable and economic operation [1]. The challenge for design of heat exchangers is to make it compact and maintain high heat transfer rate with minimum pumping power. Various heat transfer enhancement techniques have been proposed and applied in industries.

In recent years, in order to relieve the energy shortage and environmental pollutions, the energy utilization efficiency is trying to be increased for fossil energy systems. Meanwhile, a large quantity of renewable energy such as solar energy, ocean energy, etc. has been put into use. In energy conversion and power generation systems with low grade energy and renewable energy resources, miniaturization of heat exchangers can reduce the investment cost and increase the system efficiencies. For example, a heat exchanger for an ocean thermal energy conversion (OTEC) plant requires heat transfer surface area at the order of 10^4 m^2/MW [1]. In summary, high heat transfer coefficients can achieve low and uniform temperature differences in heat exchangers, increasing the exergy efficiency of the component and system.

Besides, the thermal resistance can be increased due to fouling after the long-term operation of heat exchangers, the fouling is even more serious in heat exchangers in marine applications and chemical industries. For heat exchangers with fluids of low thermal conductivity (gases and oils), the heat transfer needs to be enhanced, and it can be realized by introducing disturbance in the fluid flow (breaking the viscous and thermal boundary layers).

Liu and Sakr [2] performed a comprehensive review on passive heat transfer enhancement in pipe heat exchangers. They reviewed experimental and numerical studies on heat transfer enhancement since 2004, by using twisted tape, wire coil, swirl flow generator, etc.

The twisted tape inserts are widely adopted to enhance the heat transfer efficiency and they perform better in laminar flow regime than in turbulent flow regime [3–8]. Eiamsa-Ard et al. [3] investigated the heat transfer characteristics of turbulent flow in circular tubes with twisted tape inserts using air as the working fluid. In their work, the heat transfer performance is better with a short tape insert in entrance, compared with a long tape inserted in the tube. Guo et al. [4] conducted numerical investigation on the heat transfer behaviors in the tubes with center-cleared twisted tape or short-width twisted tape insert. Their results indicated that the flow resistance was reduced compared with the conventional tape insert. Naphon [5] experimentally studied the heat exchangers with twisted tapes inserted in the tube bundle. Correlations of flow resistance and heat transfer were obtained. Murugesan et al. [6] used V-cut twisted tape to enhance the convective heat transfer. The Nusselt numbers could be increased by increasing the depth ratios and decreasing the twist ratios and width ratios.

☆ Communicated by W.J. Minkowycz.

* Corresponding author.
E-mail address: xjl@ncepu.edu.cn (J. Xu).

http://dx.doi.org/10.1016/j.icheatmasstransfer.2014.04.018
0735-1933/

Nomenclature

BT	bare tube
D_i	inner tube diameter, m
D_o	outer tube diameter, m
f	frictional factor
h_{in}	water inlet enthalpy, J/kg
h_{out}	water outlet enthalpy, J/kg
I	current, A
k_f	water thermal conductivity, W/(mK)
k_w	stainless steel thermal conductivity, W/(mK)
L_d	developing length of the modulated flow, m
L_f	flow length between the two pressure ports, m
L_h	heating length, m
m	mass flow rate, kg/s
MHTT	modulated heat transfer tube
Nu	Nusselt number
$\Delta P_{f,m}$	measured frictional pressure drop, Pa
Pr	Prandtl number
q	heat flux on the inner wall surface, W/m^2
q_v	volume heating intensity within the wall thickness, W/m^3
Q	net heat received by water, W
Q_p	heating power, W
r	radial coordinate, m
Re	Reynolds number
ΔT	temperature difference between inlet and outlet, °C
T_b	cross-sectional average temperature, °C
T_f	water average temperature of the test section, °C
T_{in}	water inlet temperature, °C
T_{out}	water outlet temperature, °C
T_{wi}	inner wall temperature, °C
T_{wo}	outer wall temperature, °C
U	voltage, V
u	cross-sectional average velocity, m/s
x	axial coordinate, m

Greek symbols

α	local heat transfer coefficient, W/(m^{2}K)
η	thermal efficiency
ρ_l	water density, kg/m^3
φ	heat transfer enhancement ratio

Subscript

ave	average
h	heating
i	inner
m	measurements
o	outer
p	predictions
v	volume
wi	inner tube wall
wo	outer tube wall
x	axial position

Experimental correlations were achieved in their work. Eiamsa-Ard and Promvonge [7] experimentally investigated the heat transfer and pressure drop behaviors of turbulent flow in tubes with the serrated twisted tape insert. Air was used as the working fluid. The experimental results showed that the comprehensive performance was better than that with the conventional tape insert. Eiamsa-Ard et al. [8] conducted the heat transfer experiments in circular tubes with the dual twisted tape insert, showing better performance than the single twisted tape insert.

Other several passive techniques such as ribs, conical nozzle, and conical ring, are generally more efficient in the turbulent flow regime than in the laminar flow regime [9–18]. Akhavan-Behabadi et al. [9] experimentally investigated the heat transfer behaviors in heat exchangers with the coiled wires inserted in the tube bundle. In their results, the Nusselt numbers could be increased by two to three times of those in the bare tube. Promvonge [10] studied the heat transfer and friction characteristics in horizontal tubes with the square coiled wires insert. The experimental results indicated that the heat transfer and pressure drop can be augmented significantly compared with the bare tube or conventional tubes with coiled wire insert. Muñoz-Esparza and Sanmiguel-Rojas [11] numerically studied the flow and heat transfer of laminar flow in tubes with coil insert using the finite volume method. Their numerical simulations were also verified by experiments. The experimental investigation of Li et al. [12] on the heat transfer enhancement in tubes with the discrete double inclined rib insert showed that the heat transfer enhancement ratios can reach 1–1.2, with the flow resistance increased by 70–150%. Promvonge [13] investigated the heat transfer characteristics in the tubes with conical ring insert experimentally. Kongkaitpaiboon et al. [14] found that the heat transfer coefficient of turbulent flow in the tubes with the perforated conical-ring insert could be increased by 137% through experimental investigation. Promvonge and Eiamsa-Ard [15] studied the heat transfer and pressure drop characteristics in tubes with the conical nozzle and/or swirl generator insert and the experimental correlations were given. Gül and Evin's experimental research [16] on the heat transfer in tubes with the helical swirl generator inserted in the tube entrance indicated that the local heat transfer coefficients could be increased by about 20%. Jen and Yan [17] numerically investigated the heat transfer behaviors in rectangular ducts with the porous media insert. Yang and Hwang [18] studied the heat transfer characteristics in tubes with the porous media insert by numerical simulations using the k-ε turbulent flow model.

In this study a new type of heat transfer tube with mesh cylinder inserts was proposed, which is totally different technology from those reported in early literature in that the mesh cylinder is made of hollow micro-membrane with interior empty instead of bulk porous media. The mesh cylinder consists of a flat mesh screen at the bottom and a circular mesh surface on the side, dividing the tube cross section into an annular region and a core region. When the fluid flows over the mesh screen, a small portion of flow penetrates into the core region through mesh pores, while most of the fluid is within the annular region, leading to large velocity and its gradient near the wall. Preliminary experimental studies were performed to verify the idea.

2. Experimental setup and test section

Fig. 1 shows the experimental setup. The deionized/degassed water was driven by a centrifugal pump and flowed through a valve, a mass flow meter, a test section and returned to an overflow tank, which was at the atmosphere pressure. The gravitational force drove the water flow downward to the water tank at the pump tail. A heat exchanger with cooling water was used to remove the heat from the system. An overflow tube made superfluous water flowing back to the water tank, ensuring a constant water level.

The vertically arranged stainless steel tube had an outer diameter of 16.20 mm and inner diameter of 13.80 mm with a length of 2.0 m. The tube was directly heated by power source with an alternative-current (AC) voltage. The heating length was 0.98 m with two copper electrode plates welded at both ends. An electric transformer was used to convert the 380 V AC voltage to a required low voltage. The current flowing through the test tube was large due to the low electric resistance of the test tube. This heating technique was widely used in heat transfer experiments previously [19].

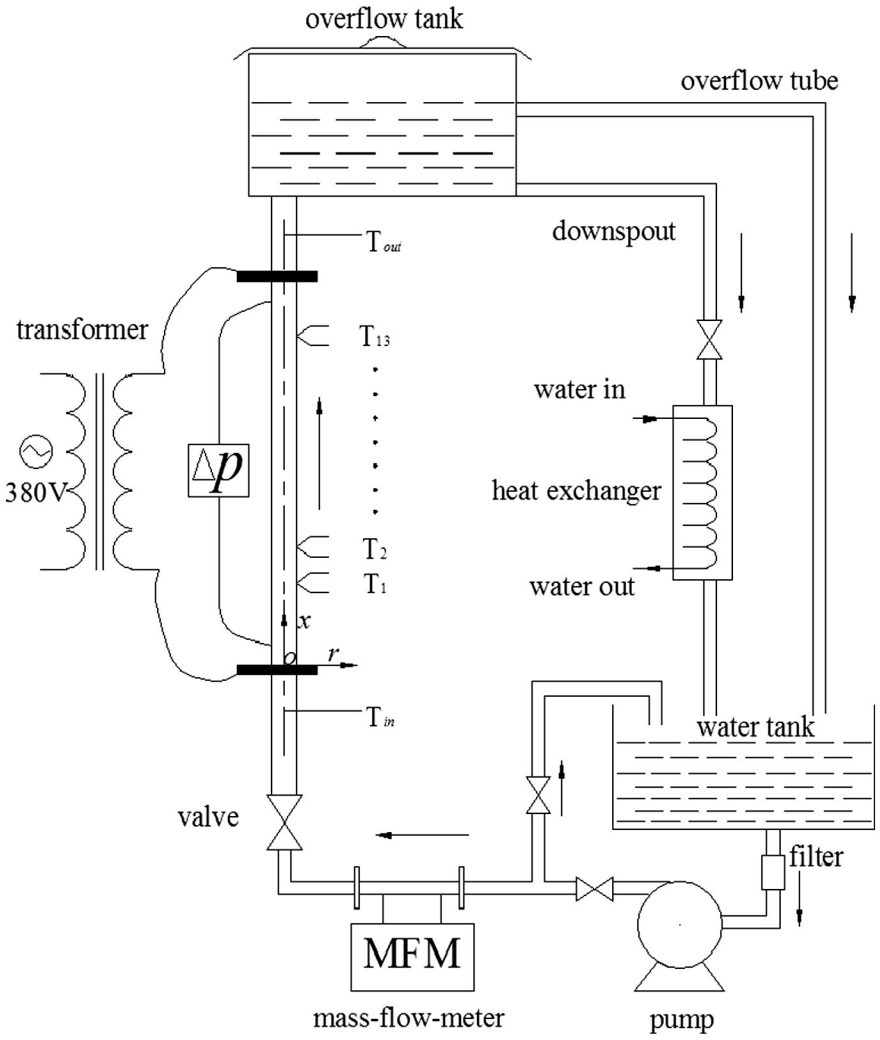

Fig. 1. The experimental setup.

A two-dimensional coordinate was established with r as the radial coordinate and x as the axial flow coordinate. The original point O ($r = 0, x = 0$) was located at the tube centerline ($r = 0$) and at the electrode plate at the bottom ($x = 0$). Thus the heating region started at $x = 0$ (bottom electrode plate) and ended at $x = 0.98$ m (the top electrode plate). Thirteen thermocouple wires were directly welded at the outer tube wall by the electric discharge technique using an instantaneous spark generation machine, thus there is little thermal resistance between the thermocouples and the tube wall. Table 1 showed the locations of thermocouples along the flow direction. The pressure drop was measured by a pressure drop transducer within a distance of 0.95 m. Two jacket thermocouples were arranged outside the heating region to measure the water inlet and outlet temperatures (T_{in} and T_{out}).

Fig. 2a shows the test tube with the dimensions. Heat transfer performance was compared between the bare tube (called BT) and the modulated heat transfer tube (called MHTT) with mesh cylinder inserted. The mesh cylinder had a flat mesh screen at the bottom and a circular mesh surface on the side, with outer diameter of 10.34 mm. The pressure-driven flow from the annular region to the core region has large flow resistance due to mesh pores, thus a large flow rate was maintained in the annular region and a small flow rate was maintained in the core region. The mesh cylinder started at $x = 0$ (the lower electrode plate). The mesh cylinder had a length of 0.98 m, which was identical to the heating length.

Fig. 2b showed the mesh screen for the mesh cylinder. The mesh wire had a diameter of 90 μm and the mesh pore had a square cross section with 150 μm on each side. Fig. 2c showed the photo of fabricated mesh cylinder.

3. Data reduction

Local and average heat transfer coefficients and Nusselt numbers were calculated based on the measured mass flow rate, water inlet and outlet temperatures, and outer wall temperatures. The received heat by the water inside the test tube was

$$Q = m(h_{out} - h_{in}) \tag{1}$$

where Q was the net heat received by water, m was the mass flow rate, h_{out} and h_{in} were the water enthalpies based on T_{out} and T_{in}, respectively.

Table 1
The locations of thermocouples along the axial flow direction (the unit is mm).

T_{in}	T_1	T_2	T_3	T_4	T_5	T_6	T_7	T_8	T_9	T_{10}	T_{11}	T_{12}	T_{13}	T_{out}
−120	15	52.5	90.0	127.0	165.0	265.0	365.0	465.0	565.0	665.0	765.0	865.0	965.0	1400

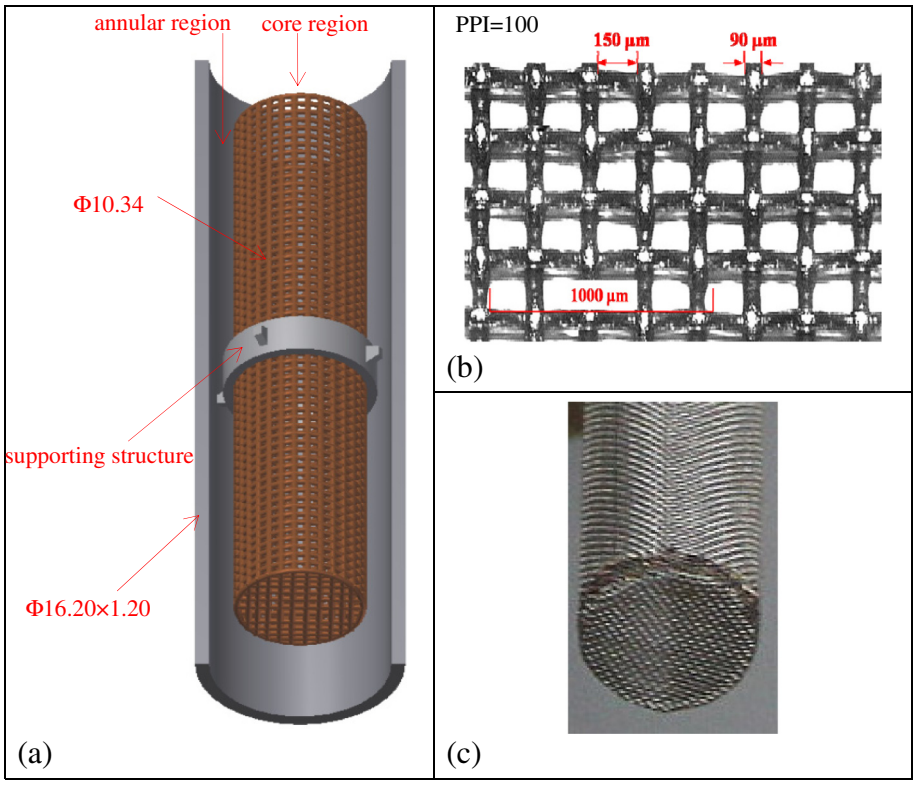

Fig. 2. The enhanced heat transfer tube with mesh cylinder inserted (a) photo of mesh screen (b) and the fabricated mesh cylinder (c).

During the experiment, the electrical heating power was $Qp = UI$, where U and I were the voltage and current from the power supply. The thermal efficiency was defined as $\eta = Q/Q_p$. It was noted that a thick thermal insulation layer was wrapped around the outer side of the tube, thus the thermal efficiency was high. The experimentally determined thermal efficiencies were in the range of 0.95–0.98 in this study.

The measured frictional factor was

$$f = \frac{2D_i \Delta P_{f,m}}{L_f \rho_l u^2} \tag{2}$$

where $\Delta p_{f,m}$ was the measured frictional pressure drop, which was the total pressure drop subtracting the gravitational pressure drop, D_i was the inner diameter, L_f was the flow length between the two pressure ports, ρ_l was the water density and u was the cross-sectional average water velocity in the tube.

The electrical resistance heating involved a volume heating intensity within the wall thickness, which was

$$q_v = \frac{4Q}{\pi(D_o^2 - D_i^2)L_h} \tag{3}$$

where D_o was the outer diameter and L_h was the heating length. The heat flux on the inner wall surface was

$$q = \frac{Q}{\pi D_i L_h}. \tag{4}$$

The calculation of heat transfer coefficient in the tube needed the inner wall temperature T_{wi}, which could be calculated by the heat conduction equation in radial direction:

$$\frac{1}{r}\frac{\partial}{\partial r}\left(rk_w \frac{\partial T}{\partial r}\right) + q_v = 0. \tag{5}$$

At $r = D_o/2$:

$$-k_w \frac{\partial T}{\partial r} = 0 (\text{Insulated wall}) \tag{6}$$

$$T = T_{wo} (\text{Measured temperature}). \tag{7}$$

Inner wall temperature T_{wi} could be calculated by solving Eq. (5) subjecting to boundary conditions in Eqs. (6) and (7) [20]:

$$T_{wi} = T_{wo} - \frac{qD_i}{4k_w} \times \frac{\left(\frac{D_i}{D_o}\right)^2 - 2\ln\left(\frac{D_i}{D_o}\right) - 1}{1 - \left(\frac{D_i}{D_o}\right)^2} \tag{8}$$

where k_w was the thermal conductivity. The local heat transfer coefficient was

$$\alpha = q/(T_{wi} - T_b) \tag{9}$$

where T_b was the cross-sectional average temperature, which had a linear function with the heating length of x. The local Nusselt number was

$$Nu = \alpha D_i / k_f \tag{10}$$

where k_f was the thermal conductivity based on local average temperature T_b. The average heat transfer coefficient within the heating length was

$$\alpha_{ave} = \frac{q}{T_{wi,ave} - T_{f,ave}} \tag{11}$$

where $T_{wi,ave} = \frac{1}{13}\sum_{x=1}^{13} T_{wi,x}$ and $T_{f,ave} = 0.5\,(T_{in} + T_{out})$. The average Nusselt number was defined based on α_{ave}, i.e., $Nu_{ave} = \alpha_{ave} D_i / k_{f,ave}$, where $k_{f,ave}$

was the thermal conductivity based on the average temperature of 0.5 ($T_{in} + T_{out}$).

For all the runs of experiment, the inlet temperature was about 30 °C. The variation ranges for some parameters were as follows: mass flow rate (m): 89–510 kg/h; heat flux (q): 41–282 kW/m^2. The Reynolds number Re ranges from 2109 to 20,175, covering the transition and turbulent flow regimes. The heating power could maintain the temperature difference either 10 °C or 20 °C ($\Delta T = T_{out} - T_{in} = 10$ or 20 °C) for each case. Almost identical operating parameters were set for BT and MHTT for comparison purpose. Table 2 summarized the running parameters for BT and MHTT (62 runs).

The mass flow meter was accurate with 0.1% resolution. The uncertainties for heat flux, temperature and pressure drops were 0.5%, 0.2 °C and 1.0% respectively. The uncertainty of heat transfer coefficient

Table 2
The runs in this study.

Runs	Tubes	m (kg/h)	q (kW/m^2)	T_{in} (°C)	T_{out} (°C)	ΔT (°C)	Re	Nu_{ave}	φ
1	BT	90.0	23.90	30.0	40.0	10.0	3203	17.89	1
2	MHTT	90.1	24.40	29.9	40.1	10.2	3209	27.92	1.56
3	BT	118.8	32.17	30.0	39.8	9.8	4240	25.43	1
4	MHTT	119.1	32.25	30.2	40.2	10.0	4262	41.20	1.62
5	BT	149.3	41.24	29.7	39.9	10.2	5297	32.96	1
6	MHTT	149.9	40.48	30.0	39.9	9.9	5337	54.26	1.65
7	BT	179.6	50.17	29.9	40.1	10.2	6398	43.93	1
8	MHTT	179.7	48.93	29.9	39.9	10.0	6389	65.99	1.50
9	BT	209.1	60.76	29.9	40.5	10.5	7491	51.82	1
10	MHTT	209.6	58.62	30.1	40.3	10.2	7497	76.28	1.47
11	BT	239.4	68.14	29.9	40.3	10.4	8548	59.55	1
12	MHTT	240.0	66.67	29.9	40.1	10.2	8548	86.13	1.45
13	BT	269.9	76.51	29.8	40.2	10.4	9617	67.07	1
14	MHTT	270.0	74.18	30.1	40.1	10.0	9636	94.58	1.41
15	BT	299.9	83.70	30.0	40.2	10.2	10,705	73.67	1
16	MHTT	299.7	81.63	30.0	39.9	9.9	10,662	103.07	1.40
17	BT	329.3	92.63	30.2	40.4	10.2	11,799	80.33	1
18	MHTT	329.2	90.08	30.1	40.1	10.0	11,746	112.00	1.39
19	BT	360.4	101.10	29.9	40.3	10.4	12,684	86.45	1
20	MHTT	360.2	98.67	30.0	40.0	10.0	12,820	120.74	1.40
21	BT	389.8	107.53	30.1	40.2	10.1	13,924	93.62	1
22	MHTT	389.8	107.33	30.1	40.2	10.1	13,923	131.09	1.40
23	BT	420.4	113.67	29.9	39.8	9.9	14,931	98.69	1
24	MHTT	420.2	114.87	30.1	40.2	10.1	15,010	138.91	1.41
25	BT	450.0	122.89	30.0	40.0	10.0	16,022	104.99	1
26	MHTT	449.9	124.23	29.9	40.0	10.1	16,011	146.23	1.39
27	BT	481.7	132.85	29.9	40.0	10.1	17,139	111.29	1
28	MHTT	481.7	133.79	29.9	40.1	10.2	17,151	152.74	1.37
29	BT	509.4	145.12	29.9	40.4	10.5	18,215	118.08	1
30	MHTT	509.5	140.98	30.0	40.1	10.1	18,152	156.40	1.32
31	BT	89.1	46.43	30.1	49.2	19.1	3475	20.09	1
32	MHTT	89.4	50.18	30.0	50.5	20.5	3522	32.59	1.62
33	BT	104.5	54.60	30.2	50.2	20.0	4720	22.86	1
34	MHTT	104.6	54.65	30.0	50.1	20.1	4123	39.95	1.75
35	BT	119.1	62.23	30.1	49.2	19.1	4643	25.72	1
36	MHTT	119.9	66.28	30.1	50.3	20.2	4724	47.37	1.84
37	BT	149.3	81.64	29.8	50.0	20.2	5860	33.51	1
38	MHTT	150.0	82.02	30.0	49.9	19.9	5889	60.98	1.82
39	BT	179.1	97.93	29.9	49.9	20.0	7018	41.42	1
40	MHTT	179.6	98.69	29.9	50.0	20.1	7040	72.70	1.75
41	BT	210.4	114.85	30.1	50.4	20.3	8288	49.80	1
42	MHTT	210.0	116.31	30.0	50.3	20.3	8259	83.50	1.68
43	BT	238.9	129.79	29.9	49.8	19.9	9351	58.30	1
44	MHTT	239.3	131.32	30.2	50.3	20.1	9427	93.87	1.61
45	BT	270.0	149.49	29.9	50.2	20.3	10,601	66.61	1
46	MHTT	270.4	148.09	30.1	50.2	20.1	10,642	103.24	1.55
47	BT	299.4	166.68	30.1	50.5	20.4	11,821	74.15	1
48	MHTT	299.7	165.16	30.1	50.3	20.2	11,797	112.92	1.52
49	BT	329.7	182.05	30.1	50.3	20.2	12,978	81.07	1
50	MHTT	329.8	181.48	30.3	50.4	20.1	13,019	122.46	1.51
51	BT	359.2	200.31	30.1	50.5	20.4	14,176	87.65	1
52	MHTT	359.2	200.21	30.1	50.5	20.4	14,182	130.27	1.49
53	BT	391.4	208.88	30.0	50.0	20.0	15,297	95.05	1
54	MHTT	391.5	215.66	30.0	50.2	20.2	15,400	142.22	1.50
55	BT	420.0	225.25	30.2	49.8	19.6	16,480	100.91	1
56	MHTT	419.8	234.58	30.2	50.6	20.4	16,588	150.55	1.49
57	BT	451.0	245.45	29.9	49.8	19.9	17,653	107.27	1
58	MHTT	450.9	252.81	30.1	50.6	20.5	17,807	160.06	1.49
59	BT	480.6	260.43	30.0	49.9	19.9	18,839	114.45	1
60	MHTT	480.5	264.40	30.1	50.3	20.2	18,922	164.45	1.44
61	BT	509.9	282.95	29.9	50.2	20.3	20,028	119.62	1
62	MHTT	510.5	282.88	30.3	50.5	20.2	20,175	169.74	1.42

Note: the heat transfer enhancement ratio was one for bare tube and larger than one for modulated heat transfer tube respectively.

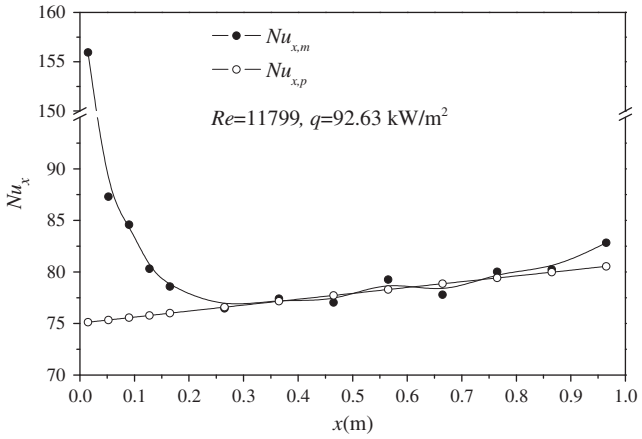

Fig. 3. Comparison of measured Nusselt numbers with the classical prediction (run17).

was a function of three independent parameters of q, T_{wi} and T_b (see Eq. (9)) and could be calculated as

$$\Delta\alpha = \sqrt{\left(\frac{\partial\alpha}{\partial q}\right)^2 \Delta q^2 + \left(\frac{\partial\alpha}{\partial T_{wi}}\right)^2 \Delta T_{wi}^2 + \left(\frac{\partial\alpha}{\partial T_b}\right)^2 \Delta T_b^2}. \quad (12)$$

Thus the relative uncertainty could be computed by substituting Eq. (9) into Eq. (12), yielding

$$\frac{\Delta\alpha}{\alpha} = \sqrt{\left(\frac{\Delta q}{q}\right)^2 + \left(\frac{\Delta T_{wi}}{T_{wi}-T_b}\right)^2 + \left(\frac{\Delta T_b}{T_{wi}-T_b}\right)^2} \quad (13)$$

where Δq, ΔT_{wi} and ΔT_b were the uncertainties of heat flux, wall surface temperature and cross-sectional average temperature respectively. The maximum uncertainty of α was obtained by low surface temperature and high bulk liquid temperature, resulting in maximum relative error of 2.39% for heat transfer coefficient.

4. Experimental results and discussion

4.1. Calibration of the experiment for bare tube

Before the formal experiment, the measured Nusselt number for turbulent flow in the bare tube was compared with the Dittus & Boelter equation [21]:

$$Nu = 0.023\mathrm{Re}^{0.8}Pr^{0.4} \quad (14)$$

where Pr was the Prandtl number. Fig. 3 showed high measured Nusselt numbers at the initial stage of heating section ($0 < x < 15$ mm), indicating the short thermal developing region. But $Nu_{x,m}$ was greatly decreased and then they were gradually increased in the fully developed regime, due to the variation of water physical property. The increasing temperature along the heating region could decrease viscosity, resulting in increasing local Reynolds numbers. The predicted results by Eq. (14) indicated by open symbol in Fig. 3 were based on the local Reynolds numbers. The measured Nusselt numbers agreed well with the classical predictions in the fully developed regime, noting that $Re = 11{,}799$ referred to the Reynolds number based on the average temperature of 0.5 ($T_{in} + T_{out}$). It was also noted that Eq. (14) was valid for the fully

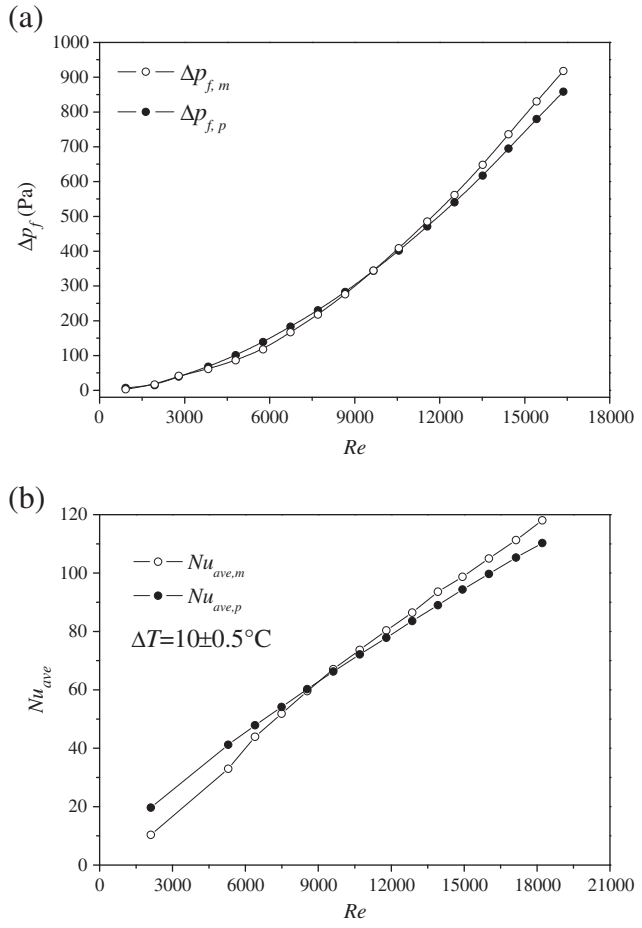

Fig. 4. Comparison of measured pressure drop and Nusselt numbers with predictions.

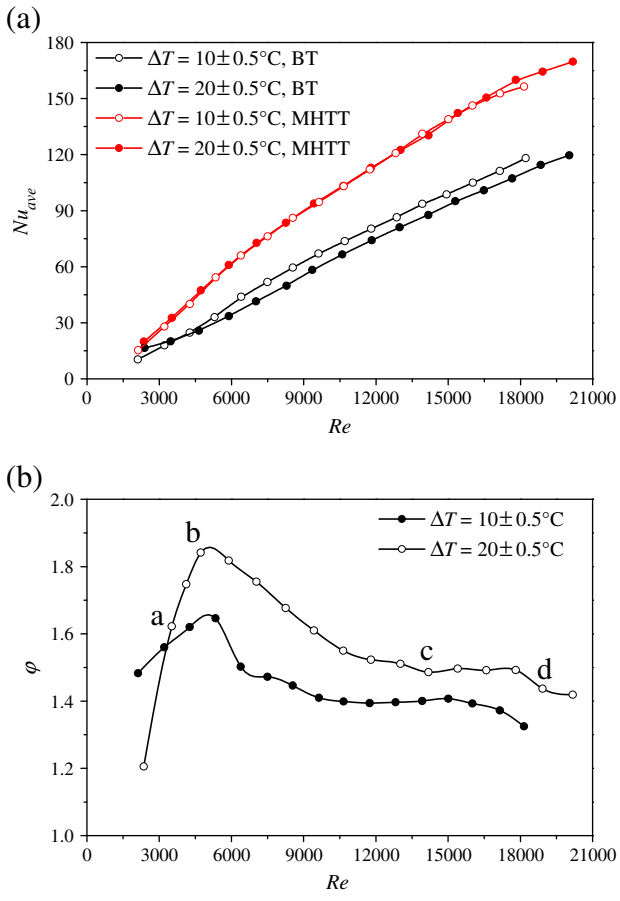

Fig. 5. The average Nusselt numbers versus Reynolds numbers (a) and heat transfer enhancement ratios versus Reynolds numbers (b).

developed heat transfer, but could not predict the heat transfer performance at the developing region at the entrance.

Fig. 4a showed the excellent agreement between measured frictional pressure drops and predicted values based on the frictional factor of $f = 64/Re$ for laminar flow and $f = 0.3164/Re^{0.25}$ for turbulent flow. The laminar flow and turbulent flow were interfaced by the transition value of $Re = 2300$. Most of the data points referred to the turbulent flow and there were only two data points belonging to the laminar flow in Fig. 4a. Fig. 4b showed the good agreement between measured average Nusselt numbers and predicted values, covering the range of $Re = 2109$–$20{,}175$. It was noted that the predicted Nusselt numbers slightly overestimated the measured values for $Re < 6000$, which was because under Reynolds number in the range of 2300–6000 the flow lied in the transition flow regime. The Dittus & Boelter equation was more suitable for the turbulent flow regime. In summary, Figs. 3, 4 proved that the experimental data were sufficiently accurate.

It was noted that the Reynolds number was defined in the same way for the bare tube (BT) and the modulated heat transfer tube (MHTT). As mentioned before, the interior of mesh cylinder was empty without porous media. In this study, the micro-membrane surface was 0.20 mm thick, resulting in only 4.26% reduction of the cross-sectional area of tube. The Reynolds number in the tube with mesh cylinder insert was only increased a little compared with that in the bare tube under the same flow rate. The large velocity and velocity gradient near the tube wall by inserting mesh cylinder was the mechanism for heat transfer enhancement, which was fulfilled by the proposed flow separation. In other words, the whole tube cross section was divided into an annular region and a core region without significant reduction of the effective cross-sectional area, which was the originality of this study.

4.2. Enhanced heat transfer with the MHTT tube

Fig. 5a showed average Nusselt number versus Reynolds number, with red and black symbols for the MHTT and BT, respectively. The MHTT significantly enhanced heat transfer. The curves for $\Delta T = 20$ °C and $\Delta T = 10$ °C were coincident with each other, indicating no effect of heat fluxes on the Nusselt numbers, where ΔT equaled to $T_{out} - T_{in}$. However, the heat fluxes affected Nusselt numbers in the bare tube. A smaller ΔT yields a "colder" water flow with larger water viscosity in the tube, thus a larger flow rate was needed to maintain the same Reynolds number for the "colder" fluid, which increased the flow turbulence as well as Nusselt number. On the other hand, when a mesh cylinder was inserted in the tube, the mass exchange took place through mesh pores, the flow turbulence caused by the mesh pores was larger than that caused by the temperature, thus there was little effect of heat fluxes on the heat transfer for MHTT. Fig. 5b showed heat transfer enhancement ratios versus Reynolds numbers. Hereby the heat transfer enhancement ratio φ was defined as the Nusselt numbers for the MHTT divided by those for the BT under the same operating conditions. With Re variation from 2109 to 20,175, the enhancement ratios were always larger than unity, indicating the heat transfer enhancement. It was noted that the transition flow regime happened in the Re range of 2300–6000. This study revealed the largest heat transfer enhancement ratio occurring at $Re = 4684$, indicating the increased turbulence intensity induced by mesh pores. Or it could be said that the inserted mesh cylinder could promote the flow to transit to turbulence flow at lower Reynolds numbers. The maximum φ reached 1.84 at $Re = 4684$. The heat transfer enhancement ratios were larger at $\Delta T = 20$ °C than those at $\Delta T = 10$ °C, indicating the increased heat transfer

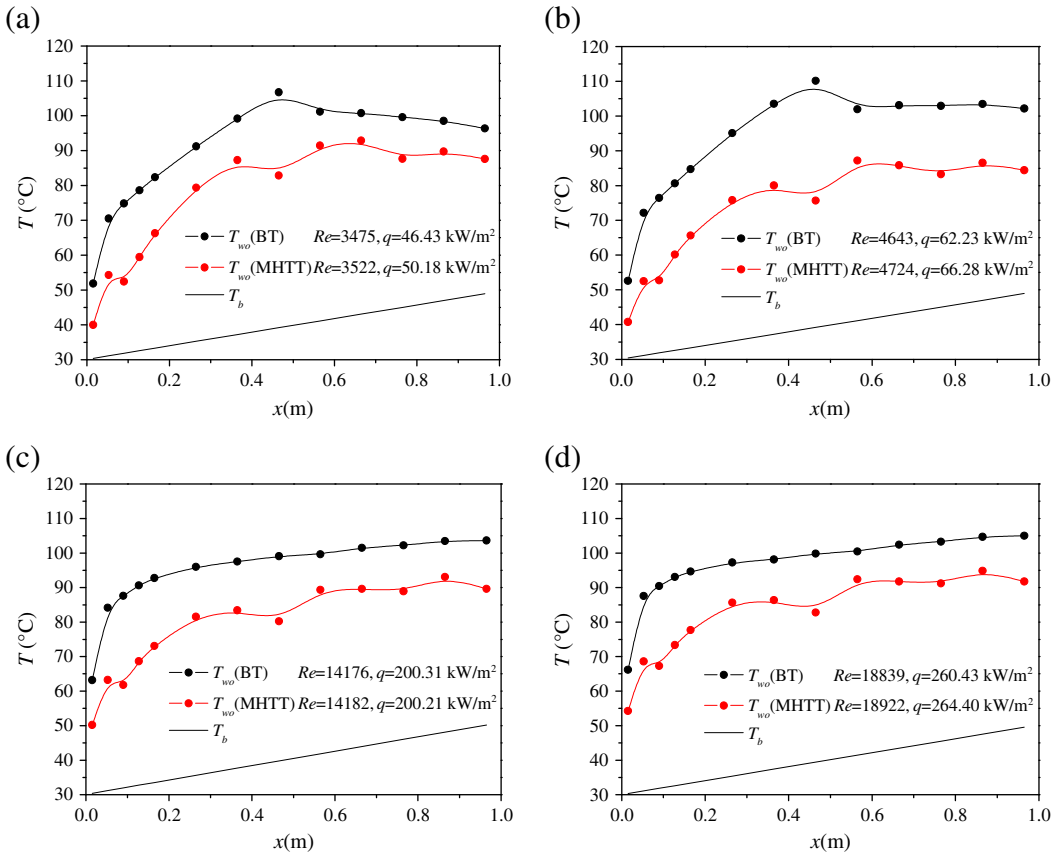

Fig. 6. Wall temperature distributions along the flow direction (a: Runs 31 and 32; b: Runs 35 and 36; c: Runs 51 and 52; d: Runs 59 and 60).

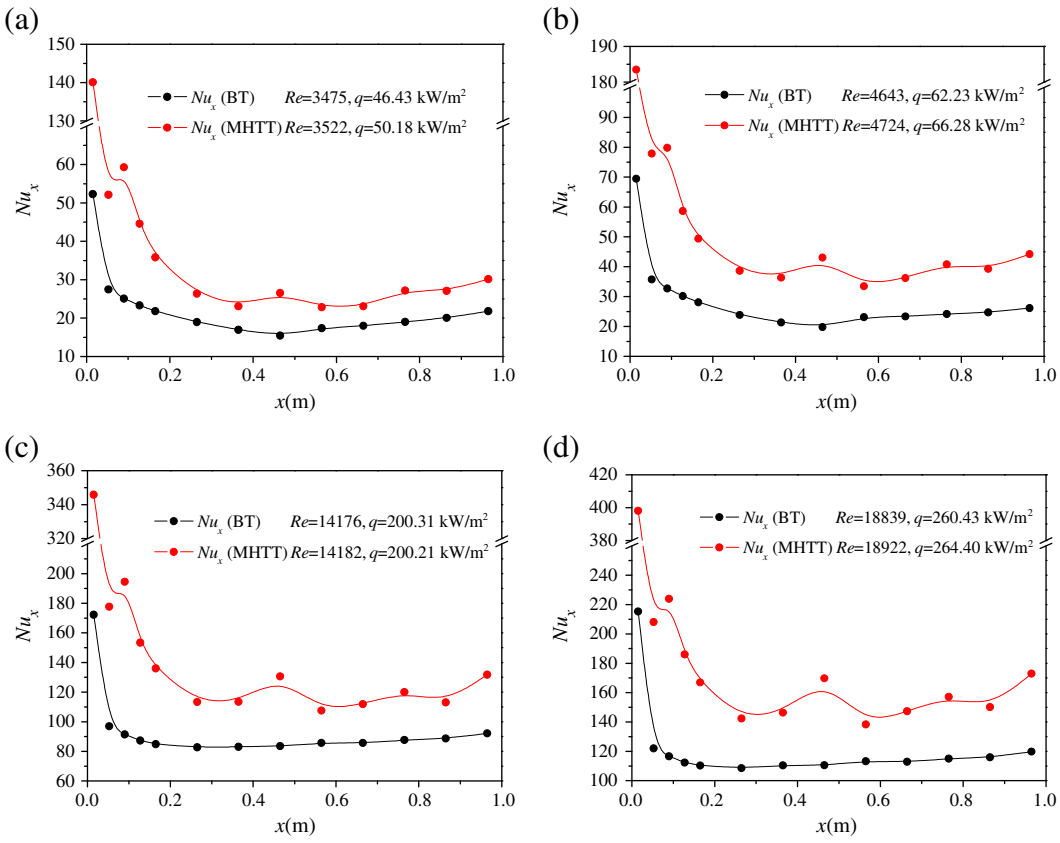

Fig. 7. Local Nusselt numbers versus axial flow direction (a: Runs 31 and 32; b: Runs 35 and 36; c: Runs 51 and 52; d: Runs 59 and 60).

enhancement at high heat fluxes. In order to further demonstrate the effectiveness of the heat transfer enhancement technique, four points of a, b, c and d were marked in Fig. 5. Each point corresponded to one case.

Fig. 6 showed the measured variations of wall temperatures (T_{wo}) along the flow direction for the four cases shown in Fig. 5. The bulk water temperature distribution was also plotted. In each subfigure of Fig. 6, at the same Re and q, T_{wo} in MHTT could be decreased by more than 8 °C than that in BT. As reported previously, the heat transfer enhancement in MHTT was more effective in the transition flow regime than that in turbulent regimes. T_{wo} in MHTT could decrease by about 20 °C at $Re = 4684$ (see Fig. 6b) than that at other Reynolds numbers (see Fig. 6a, c and d). It was noted that the supporting structure for the mesh cylinder was located at $x = 0.49$ m, where wall temperatures could be further decreased due to the interaction between the flow stream and the supporting structure.

Fig. 7 showed the variations of local Nusselt numbers along the flow direction. For the demonstrated four cases, MHTT had much higher Nusselt numbers than BT. The enhancement was more significant in the entrance region within $x < 0.2$ m. In such a short length, the Nusselt numbers for MHTT were 1.51–2.68 times higher than those for BT. The thermally developing region for MHTT was longer than that for BT. For both tubes with and without inserted mesh cylinder, the Nusselt numbers did not vary too much once the fully developed region was reached. Again, the local supporting structure had higher Nusselt numbers.

Fig. 8 showed the negligible effect of heat fluxes on the Nusselt number distribution for MHTT. The two curves for two different heat fluxes almost coincided with each other. Fig. 9 showed the total pressure drops versus Reynolds number. Pressure drops were slightly increased with increasing Reynolds numbers for BT tube, due to the small percentage of the frictional pressure drop to the total pressure drop. At low Re, such as $Re < 6000$, BT and MHTT tubes showed little difference of pressure drops. However, the slopes of pressure drops versus Re for the MHTT tube were larger than those for BT tube. Pressure drops for the MHTT were 1.08 and 1.96 times of those for BT at $Re = 4812$ and 16,364, respectively.

4.3. Explanation of the heat transfer enhancement

The proposed heat transfer tube was a typical multi-scale system (see Fig. 10a). Usually the engineering applications need macro-scale of the tube, including the tube length and diameter. Mesh pores were in the micro-scale (10–100 μm). Mass exchange through mesh pores promoted the turbulence intensity, which was regarded as one of the enhanced heat transfer mechanisms, this was why the heat transfer enhancement with the mesh cylinder insert was more significant when the flow was in transition flow regime for bare tube. In other words,

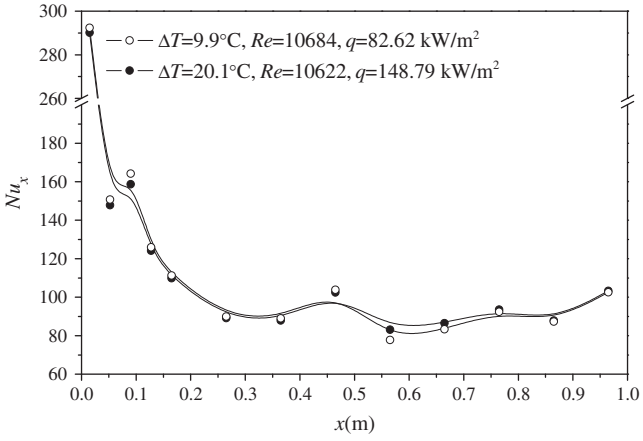

Fig. 8. Effect of heat fluxes on the local Nusselt number distribution along the flow direction (Runs 16 and 46).

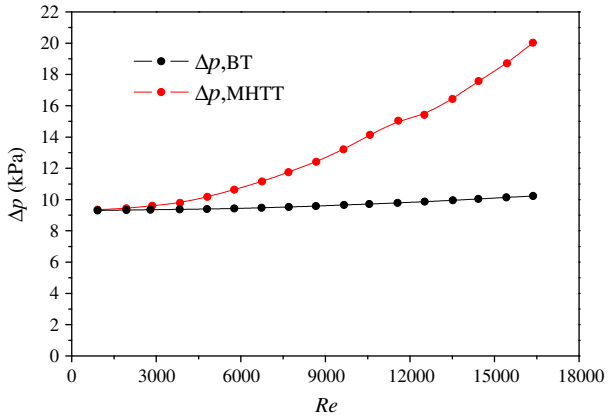

Fig. 9. The increased pressure drop with the modulated heat transfer tube.

the mesh pores of mesh cylinder promoted the turbulent flow appearing earlier. It was noted that the gap size between the tube wall and the mesh cylinder wall was in miniature scale. A limit case was considered when the mesh pore size approached zero. Under such circumstance, the mass exchange across the mesh cylinder surface was slow, and the heat transfer coefficient was inverse to the annular gap size, thus the heat transfer was significantly enhanced with a small or miniature gap size. In summary, the multi-scale characteristic of the heat transfer tube was beneficial to the heat transfer enhancement.

When a fluid stream striked an enclosed mesh cylinder with only the exit open, the micro-membrane surface provided a large flow resistance to prevent the flow from mesh cylinder inside (core region), this was why the velocity in the annular region near the tube wall was large and that in the core region was small. This mechanism has already been demonstrated by our recent studies in ref. [22]. From flow field in Fig. 10b, it could be seen that in developing region L_d of the modulated flow, water flowed continuously towards the core region of the mesh cylinder, which would decrease the velocity and velocity gradient in the annular region. Beyond the length of L_d, the velocity distribution in both the annular region and core region would not vary, and the velocity and velocity gradient were still larger in the annular region than those in the core region. This could be used to explain the heat transfer enhancement along the whole flow length in this experiment. Even though the net mass exchange across mesh pores was zero for a long tube, instantaneous mass exchange across mesh pores still existed, enhancing the turbulence intensity.

Finally, the performance evaluation criterion (*PEC*) was used to evaluate the enhanced heat transfer and increased pressure drop, which was defined as [23,24],

$$PEC = \frac{Nu_{MHTT}/Nu_{BT}}{(f_{MHTT}/f_{BT})^{1/6}}. \tag{15}$$

Fig. 11 showed the *PEC* values against the Reynolds numbers. Except in the laminar regime, PEC was always larger than one, especially under moderate Reynolds numbers. This indicated that the proposed enhanced heat transfer tube had the potential for real industrial applications after further optimization.

5. Conclusions

In this study the concept of flow field modulation was proposed. A mesh cylinder was inserted into a tube, dividing the cross section into an annular region and a core region. When a fluid stream interacted with the mesh cylinder, most of the fluid entered the annular region, leading to larger velocity and its gradient near the wall than those for the bare tube. This was believed to be the major heat transfer enhancement mechanism.

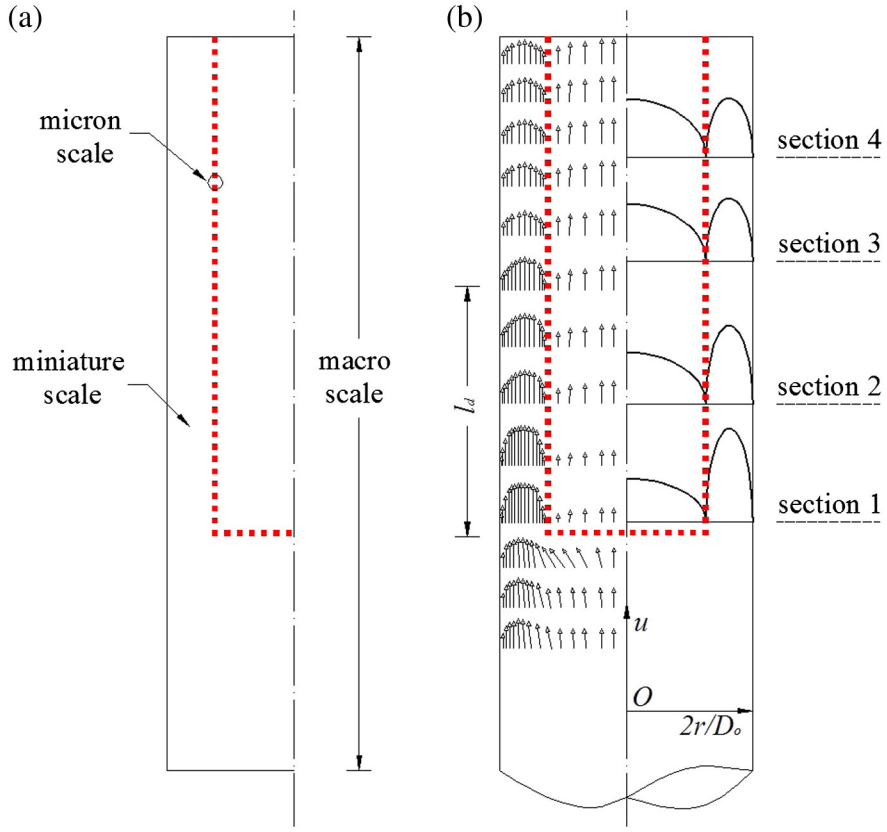

Fig. 10. The multi-scale structure of MHTT (a) and the flow field for heat transfer enhancement (b).

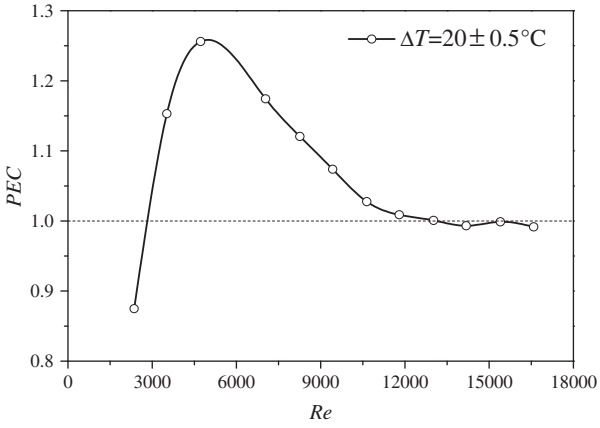

Fig. 11. The *PEC* variation against the Reynolds number.

Experiments were conducted with water as the working fluid. The tube was heated by AC current at constant heat fluxes. Reynolds numbers varied in the range of 2109–20,175 in the transition and turbulent flow regimes. The measured frictional pressure drops and heat transfer coefficients agreed well with the predictions from the classical correlations. The heat transfer enhancement ratios range from 1.21 to 1.84, with the largest value occurring in the transition flow regime. The inserted mesh screen promoted the turbulence intensity. The heat transfer enhancement mechanism could be caused by: (1) Multi-scale characteristics of the heat transfer tube; (2) Modulated flow field with larger velocity and velocity gradient near the wall; (3) Enhanced flow turbulence intensity. The detailed flow and heat transfer mechanism needed further investigation.

Acknowledgments

This work was supported by the National Basic Research Program of China (2011CB710703), the National Natural Science Foundation of China of International cooperation project (Grant No. 51210011).

References

[1] A. Dewan, P. Mahanta, K.S. Raju, P.S. Kumar, Review of passive heat transfer augmentation techniques, Proceedings of the Institution of Mechanical Engineers, Part A: Journal of Power and Energy, 2004, pp. 509–527.
[2] S. Liu, M. Sakr, A comprehensive review on passive heat transfer enhancements in pipe exchangers, Renew. Sust. Energ. Rev. 19 (2013) 64–81.
[3] S. Eiamsa-Ard, C. Thianpong, P. Eiamsa-Ard, P. Promvonge, Convective heat transfer in a circular tube with short-length twisted tape insert, Int. Commun. Heat Mass Transfer 36 (4) (2009) 365–371.
[4] J. Guo, A. Fan, X. Zhang, W. Liu, A numerical study on heat transfer and friction factor characteristics of laminar flow in a circular tube fitted with center-cleared twisted tape, Int. J. Therm. Sci. 50 (7) (2011) 1263–1270.
[5] P. Naphon, Heat transfer and pressure drop in the horizontal double pipes with and without twisted tape insert, Int. Commun. Heat Mass Transfer 33 (2) (2006) 166–175.
[6] P. Murugesan, K. Mayilsamy, S. Suresh, P.S.S. Srinivasan, Heat transfer and pressure drop characteristics in a circular tube fitted with and without V-cut twisted tape insert, Int. Commun. Heat Mass Transfer 38 (3) (2011) 329–334.
[7] S. Eiamsa-Ard, P. Promvonge, Thermal characteristics in round tube fitted with serrated twisted tape, Appl. Therm. Eng. 30 (13) (2010) 1673–1682.
[8] S. Eiamsa-Ard, C. Thianpong, P. Eiamsa-Ard, P. Promvonge, Thermal characteristics in a heat exchanger tube fitted with dual twisted tape elements in tandem, Int. Commun. Heat Mass Transfer 37 (1) (2010) 39–46.
[9] M.A. Akhavan-Behabadi, R. Kumar, M.R. Salimpour, R. Azimi, Pressure drop and heat transfer augmentation due to coiled wire inserts during laminar flow of oil inside a horizontal tube, Int. J. Therm. Sci. 49 (2) (2010) 373–379.
[10] P. Promvonge, Thermal performance in circular tube fitted with coiled square wires, Energy Convers. Manag. 49 (5) (2008) 980–987.
[11] D. Muñoz-Esparza, E. Sanmiguel-Rojas, Numerical simulations of the laminar flow in pipes with wire coil inserts, Comput. Fluids 44 (1) (2011) 169–177.
[12] X.W. Li, J.A. Meng, Z.Y. Guo, Turbulent flow and heat transfer in discrete double inclined ribs tube, Int. J. Heat Mass Transf. 52 (3) (2009) 962–970.
[13] P. Promvonge, Heat transfer behaviors in round tube with conical ring inserts, Energy Convers. Manag. 49 (1) (2008) 8–15.
[14] V. Kongkaitpaiboon, K. Nanan, S. Eiamsa-ard, Experimental investigation of heat transfer and turbulent flow friction in a tube fitted with perforated conical-rings, Int. Commun. Heat Mass Transfer 37 (5) (2010) 560–567.
[15] P. Promvonge, S. Eiamsa-ard, Heat transfer enhancement in a tube with combined conical-nozzle inserts and swirl generator, Energy Convers. Manag. 47 (18) (2006) 2867–2882.
[16] H. Gül, D. Evin, Heat transfer enhancement in circular tubes using helical swirl generator insert at the entrance, Int. J. Therm. Sci. 46 (12) (2007) 1297–1303.
[17] T.C. Jen, T.Z. Yan, Developing fluid flow and heat transfer in a channel partially filled with porous medium, Int. J. Heat Mass Transf. 48 (19) (2005) 3995–4009.
[18] Y.T. Yang, M.L. Hwang, Numerical simulation of turbulent fluid flow and heat transfer characteristics in heat exchangers fitted with porous media, Int. J. Heat Mass Transf. 52 (13) (2009) 2956–2965.
[19] D. Yang, J. Pan, C.Q. Zhou, X.J. Zhu, Q.C. Bi, T.K. Chen, Experimental investigation on heat transfer and frictional characteristics of vertical upward rifled tube in supercritical CFB boiler, Exp. Thermal Fluid Sci. 35 (2) (2011) 291–300.
[20] H. Bas, V. Ozceyhan, Heat transfer enhancement in a tube with twisted tape inserts placed separately from the tube wall, Exp. Thermal Fluid Sci. 41 (2012) 51–58.
[21] F.W. Dittus, L.M.K. Boelter, Heat transfer in automobile radiators of the tubular type, Int. Commun. Heat Mass Transfer 12 (1) (1985) 3–22.
[22] Z. Cao, J.L. Xu, D.L. Sun, J. Xie, F. Xing, Q.C. Chen, Numerical simulation of modulated heat transfer tube in laminar flow regime, Int. J. Therm. Sci. 75 (2014) 171–183.
[23] J.F. Fan, W.K. Ding, J.F. Zhang, Y.L. He, W.Q. Tao, A performance evaluation plot of enhanced heat transfer techniques oriented for energy-saving, Int. J. Heat Mass Transf. 52 (1) (2009) 33–44.
[24] X. Zhang, Z. Liu, W. Liu, Numerical studies on heat transfer and flow characteristics for laminar flow in a tube with multiple regularly spaced twisted tapes, Int. J. Therm. Sci. 58 (2012) 157–167.